HHS Public Access

Author manuscript

Exp Physiol. Author manuscript; available in PMC 2019 April 01.

Published in final edited form as:

Exp Physiol. 2018 April 01; 103(4): 590–603. doi:10.1113/EP086818.

Aortic Dysfunction in Metabolic Syndrome Mediated by Perivascular Adipose Tissue TNFα and NOX2 Dependent Pathway

Evan DeVallance[1], **Kayla W Branyan**[1], **Kent Lemaster**[2], **I. Mark Olfert**[1], **David M. Smith**[3], **Emidio E Pistilli**[1], **Jefferson C Frisbee**[2,4], and **Paul D. Chantler**[1]

[1]Division of Exercise Physiology, West Virginia University School of Medicine, Morgantown, WV

[2]Department of Physiology and Pharmacology, Schulich School of Medicine and Dentistry, University of Western Ontario, London, ON, Canada

[3]Department of Biochemistry, West Virginia University School of Medicine, Morgantown, WV

[4]Department of Medical Biophysics, Schulich School of Medicine and Dentistry, University of Western Ontario, London, ON, Canada

Abstract

Aims—Perivascular adipose tissue (PVAT) is recognized for its vaso-active effects, however it's unclear how Metabolic Syndrome impact thoracic-aorta (t)PVAT and the subsequent effect on functional and structural aortic stiffness.

Methods & Results—Thoracic aorta and tPVAT were removed from 16–17 week old lean (LZR, n=16) and obese Zucker (OZR, n=16) rats. OZR presented with aortic endothelial dysfunction, assessed by wire-myography, and increased aortic stiffness, assessed by elastic modulus. OZR-tPVAT exudate further exacerbated the endothelial dysfunction reducing nitric oxide and endothelial dependent relaxation ($p<0.05$). Additionally, OZR-tPVAT exudate had increased MMP9 activity ($p<0.05$) and further increased elastic modulus of the aorta following 72-hours of coculture ($p<0.05$). We found the observed aortic dysfunction caused by OZR-tPVAT was mediated through increased production and release of TNFα ($p<0.01$), which was dependent on tPVAT NADPH-oxidase 2 (NOX2) activity. OZR-tPVAT ROS and subsequent aortic dysfunction

Corresponding author: Paul D Chantler, One Medical Center Drive, Morgantown, WV, 26505, pchantler@hsc.wvu.edu, tel: (304) 293-0646, fax: (304) 293-7105.

Conflicts of Interest

The authors declare no conflicts of interest.

Author Contributions

Terminal animal procedures and experiments were conducted in Paul Chantler's laboratory in the School of Medicine at West Virginia University.

ED: Conceptual design, data collection, analysis, interpretation, writing and revising of the manuscript.
KWB: Data collection, analysis, and manuscript revisions
KM: Data collection, analysis, and manuscript revisions
IMO: Conceptual design and revising of the manuscript
DMS: Conceptual design, interpretation, and revising of the manuscript
EEP: Conceptual design and revising of the manuscript
JCF: Conceptual design, interpretation, and revising of the manuscript
PDC: Conceptual design, interpretation, and revising of the manuscript

was inhibited by TNFα neutralization and/ or inhibition of NOX2. Additionally, we found OZR-tPVAT had reduced activity of the 20S proteasome's active sites ($p<0.05$) and reduced superoxide dismutase activity ($p<0.01$).

Conclusion—Metabolic syndrome causes tPVAT dysfunction through interplay between TNFα and NOX2 leading to tPVAT mediated aortic stiffness by activation of aortic ROS and increased MMP9 activity.

Keywords

Perivascular adipose tissue; metabolic syndrome; tumor necrosis factor alpha

Introduction

A clustering of cardiovascular risk factors, known as metabolic syndrome (MetS), is associated with increases in oxidative stress and inflammation leading to vascular dysfunction (Katakam *et al.*, 2006; Donley *et al.*, 2014; Brooks *et al.*, 2015). In MetS, the aorta becomes less compliant through an increase in both functional and structural stiffness. Functional stiffness arises from reduced nitric oxide (NO) bioavailability increasing smooth muscle tone and redistributing circumferential stress onto the extracellular matrix (ECM) (Wilkinson *et al.*, 2004). The remodeling of the ECM, fragmentation of elastin and deposition of collagen, is the hallmark of structural stiffness (Fitch *et al.*, 2001; Lakatta & Levy, 2003). The resulting loss of aortic compliance increases afterload on the heart (O'Rourke, 1990), reduces coronary perfusion (Lakatta & Levy, 2003), and increases pulsatile flow to the periphery (Levy *et al.*, 2001), which can ultimately lead to end organ damage (Saji *et al.*, 2012).

Perivascular adipose tissue (PVAT) surrounds much of the vasculature and has various phenotypes and function depending on location. Over the past decade, PVAT has been shown to actively regulate vascular function. Unlike other PVAT depots, "brown-like" thoracic (t)PVAT encases the aorta and releases vasoactive factors, which promote beneficial vascular effects through the promotion of NO production (Gao *et al.*, 2007). In disease states, PVAT becomes dysfunctional and shifts towards a pro-oxidative and pro-inflammatory state (Chen *et al.*, 2013; Mikolajczyk *et al.*, 2016). Recently, in both human and mouse visceral adipose tissue, proteasome function was linked to tissue dysfunction (Diaz-Ruiz *et al.*, 2015), which may promote ubiquitin mediated inflammation (Ghosh *et al.*, 2015). This potential mechanism of adipose dysfunction and inflammation is currently unexplored in PVAT. Of particular interest is the cytokine tumor necrosis factor alpha (TNFα), which has a potent vasoactive effect, induces the production of inflammatory cytokines, including its own transcription (Chen *et al.*, 2004; Parameswaran & Patial, 2010), and activates the production of ROS from oxidative enzymes, such as NADPH oxidase (Chen *et al.*, 2004; Kim *et al.*, 2007). Data from peripheral PVAT depots highlight the detrimental impact of a pro-oxidative and pro-inflammatory state on small artery function (Greenstein *et al.*, 2009; Virdis *et al.*, 2015), especially endothelial dependent dilation (EDD). Studies show pathological ECM remodeling and arterial stiffness is mediated through reductions in NO and EDD (Jenkins *et al.*, 1998; Gurjar *et al.*, 1999; Fitch *et al.*, 2001). These previous studies highlight the effects of individual disease states, but the effect

of the concurrent risk factors in MetS on tPVAT function is limited. However, much of the current MetS literature on PVAT function is in depots surrounding mesenteric or small resistant arterioles. Significant aortic dysfunction has been previously shown in a rat model of MetS, the obese Zucker rat (Mingorance *et al.*, 2009). However, it remains unknown to what extent tPVAT affects the pathological changes in MetS and how it regulates aortic function, which is key to understanding the vascular consequences of MetS and developing effective therapeutics. Thus, this study aimed to uncover key pathways, which drive tPVAT dysfunction and the subsequent mediators of aortic impairment in MetS. We hypothesize phenotypic shifts in MetS tPVAT leads to an increase in ROS production from TNFα activation of NOX2. We further hypothesize tPVAT derived pro-inflammatory cytokines activate ROS production in the aorta diminishing NO bioavailability with subsequent aortic dysfunction.

Methods & Materials

Ethical Approval

Zucker rats from Envigo were used to conduct the experiments reported in this manuscript on an approved protocol by the West Virginia University Health Science Center (WVUHSC) Animal Care and Use Committee, which meets the NIH guidelines for care and use of laboratory animals and complies with the animal use ethics checklist set forth by the Journal of Experimental Physiology.

Animals

Male lean (LZR) and obese (OZR) Zucker rats were purchased from Envigo Laboratories at 8–9 weeks of age (n=16/group). Animals were housed at the WVUHSC animal care facility and received standard chow and tap water ad libitum. At time of terminal procedures 16–17 weeks old animals were weighed then deeply anesthetized by IP injection of pentobarbital sodium (50 mg/kg) and tracheal was intubated to aid in keeping a patent airway. All rats then received carotid artery and jugular vein cannulation to measure mean arterial pressure and to administer heparin, respectfully. Animals were then euthanized via severing of the diaphragm and subsequent removal of the aorta, which was placed in ice cold Krebs Henseleit Buffer (1.18 mM KH_2PO_4, 1.2 mM $MgSO_4$•$7H_2O$, 4.7 mM KCl, 25 mM $NaHCO_3$, 118 mM NaCl, 5.5 mM glucose, 0.026 mM Ethylenediaminetetraacetic acid (EDTA), 2.5 mM $CaCl_2$•$2H_2O$, bubbled with 95% O_2). tPVAT was then carefully removed from the aorta under a dissecting microscope, and the aorta was cut into 3mm rings and tPVAT were portioned out to examine gene expression, inflammatory mediators and its role on aortic function.

Gene Expression

50mg sections of tPVAT were incubated at 37°C in physiological HEPES buffer (43.7 mM NaCl, 80 mM KCl, 1.17 mM $MgSO_4$•$7H_2O$, 1.6 mM NaH_2PO_4, 18 mM $NaHCO_3$, 0.03 mM EDTA, 5.5 mM glucose, 5 mM HEPES) or HEPES buffer containing 4μM TNFα neutralizing antibody (TNFα-AB, Catalog #: AF-510-NA, R&D systems) at a ratio of 200μg/mL. After 1 hour PVAT was removed and snap frozen. To assess gene expression, tPVAT was homogenized in QIAzol and processed for qPCR using the RNeasy Lipid Tissue

MiniKit (Qiagen), QuantiTect reverse transcription kit (Qiagen 205313). Equal concentrations of cDNA were then loaded into the QIAgility (Qiagen), which mixed 20μL PCR reactions with QuantiTect primer assays [Adiponectin (QT01169343), β-actin (QT00193473), catalase (QT00182700), CCL5 (QT01083614), CCR3 (QT00183925), CCR5 (QT01084034), CD4 (QT00181811), CD68 (QT00372204), CD8a (QT00177261), GSR (QT01083285), IFN-γ (QT00184982), IL-10 (QT00177618), IL-13 (QT00184842), IL-1β (QT00181657), IL-4 (QT01590316), Keap1 (QT00189595), MMP2 (QT00996254), MMP9 (QT00178290), $Gp91^{phox}$ (QT00195300), Nrf2 (QT00183617), p47phox (QT00189728), SOD-1 (QT00174888), SOD2 (QT00185444), TIMP-1 (QT00185304), TNF (QT02488178), TSP-1 (QT01300607), UCP-1 (QT00183967), Qiagen] and QuantiFast Sybr Green Master Mix (Qiagen 204056). Relative quantification was carried out by the 2^(ddCt) method compared to the control gene β-actin, with the reciprocal used for graphical representation of negative fold changes.

Measurement of ROS

Dihydroethidium (DHE, Invitrogen D1168) assays were performed on unfixed aortic rings and tPVAT sections to evaluate ROS production. Aortic rings were placed in a 96-well plate containing 200μl HEPES buffer with the following treatments: control (no drug), tPVAT, Crossover tPVAT (i.e., LZR-tPVAT on OZR aortic rings and OZR-tPVAT on LZR aortic rings), apocynin (10μM, Millipore, Calbiochem 178385-1GM), NOX2ds-TAT (50μM, Applied Biosystem Inc), or 4-Hydroxy-TEMPO (TEMPOL 100μM, Sigma-Aldrich 176141) at 37°C. Additionally, tPVAT was pretreated, with Pyrogallol (10μM, MP Biomedical 151993), NOX2ds-TAT (50μM), or TNFα-AB (4μM). Aortic rings were incubated in drug treatment for 30 minutes followed by addition of DHE to 10μM and incubated for another 30 minutes. Following completion of DHE incubation samples were washed in HEPES buffer, placed in Optimal Cutting Temperature compound (OCT, Fisher Healthcare™) and frozen in liquid nitrogen cooled isopentane and stored at −80°C. DHE OCT blocks were cut into 8μm slices using a cryostat and transferred to charged slides (Fisherbrand® Superfrost®) and stained/mounted with DAPI mounting media (Vector laboratories). Slides were imaged with an EVOS fluorescent microscope (Invitrogen EVOS FL Auto Cell Imaging System, RFP light cube ex:531/40em:593/40), 3 image per treatment, were analyzed by ImageJ as fluorescent density/nucleus, the mean of the 3 images/treatment were used as the mean for each animal. Values were normalized to signal from tempol treatment to eliminate background signal.

NO Bioavailability

Aortic NO production was measured according to manufacturer's instructions by 4-Amino-5-Methylamino-2′,7′-Difluorofluorescein-Diacetate (DAF-FM-DA Invitrogen). 3mm aortic rings were placed in individual wells of a 96-well plate containing 200μl of HEPES buffer supplemented with L-Arginine (100μM, MP Biomedical Inc. 100736), with the following treatments: control (no added drug), tPVAT, Crossover tPVAT, tPVAT+TNFα-AB (4μM) or nitro-L-argininemethylester (L-NAME, an inhibitor of NO synthase, Sigma-Aldrich N5751). After 30-minutes incubation with treatment DAF-FM-DA 10μM was added and the vessel was stimulated with methacholine (MCh, 1×10^{-6} Sigma-Aldrich A2251). After 10 minutes, rings were removed and conditioned solution was read in a plate reader

(BioTek Synergy HT) excitation/emission at 495/515nm wavelength. Fluorescence was normalized to aorta length and L-NAME value.

PVAT Cytokine Profile

tPVAT (200mg/mL) was incubated in HEPES buffer for 2 hours at 37°C. The tPVAT was removed and the media was snap frozen and stored at −80°C. The conditioned media was run on rat inflammatory panel-2 (Mesoscale discovery V-plex K15059D-2), MMP9 activity ELISA (GE Biotrak activity assay RPN2634), and high molecular weight adiponectin ELISA (Mybiosource MBS020496). Additionally, tPVAT homogenates were run on inflammation rat panel-1 (Mesoscale discovery K15179C-9), 20S proteasome ELISA (Mybiosource MBS730715), and Ubiquitin ELISA (Mybiosource MBS039103). All assays were run per the manufacturer's instructions.

PVAT Tissue Function

tPVAT homogenates were run per manufacturer's instructions for SOD activity (Sigma-Aldrich 19160-1KT-F), total and phosphorylated NF-κBp65 (ThermoFisher ThermoFisher multispecies InstantOne™ ELISA Kit, 85-86083-11). tPVAT homogenized in HEPES buffer containing 1mM DTT, 2mM ATP, and 10mM magnesium chloride were assayed with 100μM LLVY-AMC (ENZO BML-P802-0005), 100μM nLPnLD-AMC (Bachem I-1850.0005), and 10μM RLR-AMC (Boston Biochem S-290) these substrates are cleaved by the three different protease sites in the 20S core particle, and are thus a good general indicator of proteasome degradation capacity in the cell. Proteasome assays were measured by kinetic read (1read/minute for 120 minutes) on plate reader (ex/em 380/460nm) warmed to 37°C. V-max for each assay was determined from 30 points on the linear portion of the kinetic read and normalized to V-max in the presence of the 20S inhibitor MG132.

Aortic Reactivity

3mm thoracic aortic rings (cleaned of surrounding tissue, n=14–16) were rinsed in physiological salt solution and mounted in a myobath chamber between a fixed point and a force transducer (World Precision Instruments) and pre-stretched to equilibrate for 1 hour in Krebs Henseleit Buffer aerated with 95%O_2 and 5%CO_2 at 37°C. After equilibration, aortic baseline tension was adjusted to 1 gram and vessel viability was checked with 50mM of KCl and rings not generating a rapid response were excluded from the study. To test EDD, aortic rings were pre-constricted with phenylephrine (PE, 1×10^{-7}M Sigma-Aldrich P6126) and a stable tension was reached and recorded followed by increasing doses of MCh (1×10^{-9}M–1×10^{-5}M). Relaxation was calculated as %relaxation for each dose of MCh from the following equation:

$$\%\ \text{relaxation} = \left(\frac{Z-x}{Z-y}\right)\times 100,$$

where z=tension after PE 1×10^{-7}M, x=tension following a given does of MCh, and y=baseline tension.

Following the relaxation curve, the system was washed again and allowed to return to baseline. To test the effect of tPVAT on EDD, tPVAT exudate and exudate generated after treatment with TNFα-AB and/or NOX2ds-TAT was either snap frozen and used in crossover experiments or used immediately. Exudate was added to the bath and rings incubated for 30 minutes. Additionally, a subset of rings was incubated with the NO inhibitor L-NAME and underwent relaxation experiments both with and without tPVAT present. Pilot studies showed no difference in EDD between exudate vs. tPVAT tissue incubation. Following the incubation, relaxation curves was carried out as described above. Aortas were treated with both NOX2ds-TAT and TNF-AB to assess the direct impact of these drugs on the aorta. Finally, aortic rings both with and without tPVAT incubation were pre-constricted with PE 1×10^{-7}M and treated with increasing doses of sodium nitroprusside (SNP; 1×10^{-9}M–1×10^{-5}M, MP Biomedical 152061).

Aortic Stiffness via Elastic Modulus

Aortic rings were incubated in Ca^{2+} free Van Breemen solution (119 mM NaCl, 4.7 mM KCl, 1.17 $MgSO_4$•$7H_2O$, 20 mM $MgCl_2$•$6H_2O$, 1.18 mM NaH_2PO_4, 24 mM $NaHCO_3$, 0.03 mM EDTA, 2mM ethylene glycol-bis (β-aminoethyl ether)-N,N,N′,N′-tetraacetic acid (EGTA), 5.5 mM glucose) to elicit a passive state and mounted on an automated motorized force transducer (Aurora Scientific Inc. model-6350*358) and force output was recorded in lab chart software by powerlab (AD instruments). Rings were pre-conditioned by a 20 mN 1-minute stretch and then all tension was removed (i.e. force = 0 mN). Rings were then stretched to 10mN of force for 3 minutes and the internal diameter and wall thickness were measured. Subsequently, the automated force transducer increased the aortic ring diameter by 25% of initial internal diameter every 3 minutes until mechanical failure. Stress and strain equations were modified from those previously used (Brooks *et al.*, 2015) to match those used in large arteries (Fleenor *et al.*, 2014) and the slope of the stress-strain curve is used to determine the elastic modulus. Stress and strain were calculated as follows:

$$\text{one-dimensional stress}(t) = \lambda L/2HD\,.$$
$$\text{strain}(\lambda) = (\Delta d/d(i)\,.$$

Δd=change in diameter, d(i)=initial diameter) L=one-dimensional load applied, H=wall thickness, and D=length of vessel.

PVAT Culture Studies

To determine the direct impact of PVAT on mechanical stiffness, LZR aortic rings (n=4rings/treatment) were cultured for 72-hours in RMPI + GlutaMAX™ + 25 mM HEPES media (gibco® by Life Techonologies™) with streptomycin and kept in a CO_2 cell incubator at 37°C under 5% CO_2, under the following conditions; control (just media), LZR PVAT, OZR PVAT, or OZR PVAT+TNFα-AB (4μM). For these experiment 4 aortic ring segments was taken from an LZR and placed in separate wells of a 6 well culture dish with 5ml of media and 3 wells received 200mg of tPVAT from one of the conditions listed above. Media was discarded and replenished daily. Following the 72-hours of culture aortic rings were subjected to the protocol described above to generate an elastic modulus.

Statistics

All data is represented as means ± standard deviation. All experiments were run in duplicate, and the reads averaged for each animal. Data analysis and graphing were conducted using GraphPad Prism 6 software and $p<0.05$ was set as the mark for statistical significance. Comparisons between LZR and OZR were conducted using a simple student T-test, while repeated measure ANOVA analysis was used for treatment effects, effect of tPVAT, and aortic ring relaxation, with Tukey post hoc test for multiple comparisons. Aortic relaxation, NO, and ROS data from the aorta alone (Ao) and aorta with tPVAT (Ao-tPVAT) first displayed in figure 1 are shown again in subsequent figures as a point of reference and do not depict a new set of experiments.

Results

Animal Characteristics

As expected OZR presented with increased weight ($p<0.05$, OZR 604± 28g vs LZR 419± 40g), mean arterial blood pressure ($p<0.05$, OZR 135± 15mmHg vs LZR 106± 4mmHg), blood glucose ($p<0.05$, OZR 184± 30mg/dl vs LZR 98± 16mg/dl), triglycerides ($p<0.05$, OZR 124± 20mg/dl vs LZR 25± 9mg/dl).

tPVAT Mediated Aortic ROS Production—ROS production was higher in OZR aorta compared to LZR ($p<0.05$, Fig. 1A). We then incubated the LZR aorta with LZR tPVAT and identified a slight non-significant reduction in ROS production. In contrast, when the OZR aorta was incubated with OZR tPVAT, aortic ROS production was increased by ~120% ($p<0.001$, Fig. 1A). Further, the activation of aortic ROS production was significantly inhibited when the OZR aorta was treated with apocynin, and to a lesser extent with NOX2ds-TAT (Fig. 1A). The SOD activity in the OZR aorta was diminished compared to LZR ($p<0.001$, Fig. 1B). The increased ROS production has the potential to impact NO production and EDD.

tPVAT Effect on NO and Aortic Relaxation—The aortic EDD (without the presence of tPVAT) in OZR was blunted by ~15% in comparison to LZR EDD ($p<0.01$, Fig. 1C). In the OZR, tPVAT further blunted aortic EDD by ~10% ($p<0.01$) compared to OZR without tPVAT (Fig. 1C). In contrast, LZR aortic EDD in the presence of LZR-tPVAT improved EDD by 5% ($p<0.05$, Fig. 1C). Treatment of the aorta with the L-NAME removed the effects of both LZR and OZR tPVAT (Fig. 1D). Importantly, endothelial independent dilation to SNP was not different between the two groups in the presence or absence of tPVAT ($p>0.05$, maximal relaxation: LZR Ao 101±2%, LZR tPVAT-Ao 100±5%, OZR Ao 98±6%, OZR tPVAT-Ao 97±14%). As expected, we found reduced NO bioavailability in the aorta from OZR compared to LZR (Fig. 1F). Adding to this known finding, we showed aortic NO production was further reduced by ~20% ($p<0.01$) in the presence of OZR-tPVAT (Fig. 1F). In contrast, LZR-tPVAT increased ($p<0.05$) aortic NO production in the LZR by ~15% (Fig. 1F). These data illustrated tPVAT caused further impairment in OZR aortic EDD. We then wanted to determine if this was due to the release of cytokines from tPVAT or, in part, due to intrinsic properties of the OZR aorta. To assess this, we preformed crossover experiments were the LZR aorta was exposed to OZR-tPVAT media and vice versa.

PVAT Crossover Treatments—First we explored the effect of crossover tPVAT treatment on aortic ROS production. Interestingly, the LZR "healthy" aorta was not protected against OZR-tPVAT activation of aortic ROS production ($p<0.001$, Fig. 1E). Additionally, LZR-tPVAT was treated with pyrogallol to produce ROS. LZR-tPVAT with pyrogallol increased ROS production (Fig. 1E) and decreased EDD from the LZR aorta ($p<0.05$, max relaxation: LZR tPVAT+ pyrogallol-Ao 74±7% vs LZR tPVAT-Ao 87±4.2%) but not to the same extent as OZR-tPVAT ($p<0.05$, max relaxation: LZR tPVAT+ pyrogallol-Ao 74±7% vs OZR tPVAT-LZR Ao 64±5%). We then incubated LZR-tPVAT with the OZR aorta, which reduced aortic ROS production ($p<0.01$, Fig. 1E). Whereas, when OZR-tPVAT was incubated with the LZR aorta NO production was reduced, with subsequently impaired aortic EDD ($p<0.01$) in the LZR (Fig. 1 F&G). Conversely, the crossover treatment improved ($p<0.01$) NO production and aortic EDD in OZR treated with LZR-tPVAT (Fig. 1 F&G).

tPVAT Environment

Gene Expression—To assess the effect of MetS on the tPVAT environment we first compared gene expression of key transcripts involved in adipose phenotype, pro/anti-inflammatory cytokines, and pro & anti-oxidants. OZR showed a significant drop in uncoupling protein-1 (UCP-1) expression suggesting a shift towards a "whiter" phenotype ($p<0.01$, Fig. 2A) and increased immune cell markers CD68 (macrophages, $p<0.05$) and CD8a (cytotoxic T-cells, $p<0.05$) (Fig. 2A). This was accompanied by an increased expression of pro-inflammatory/oxidative genes (Fig. 2B). We also identified a reduction in gene expression of the protective anti-inflammatory/oxidant genes, which could exacerbate the pro-inflammatory/oxidative changes of tPVAT from OZR's (Fig. 2C). With the observed increase in oxidative gene expression we sought to measure ROS production and SOD activity in tPVAT.

tPVAT Function—ROS was significantly increased in OZR-tPVAT compared to LZR-tPVAT ($p<0.001$, Fig. 3A), in part, due to a reduced SOD activity in OZR-tPVAT ($p<0.001$, Fig. 3B). With the sizable increase in ROS production we were interested in the clearance of damaged cellular components. We found proteasome activity was globally diminished in OZR-tPVAT. This was shown by reduced ($p<0.01$) V-max across all 3 assays: LLVY, RLR, and nLDnLP (chymotrypsin-like, trypsin-like, and peptidylglutamyl-peptide hydrolyzing active sites) (Fig. 3C). This proteasome dysfunction was again highlighted by an increased expression of ubiquitin, suggesting a reduced ability to clear ubiquitinated proteins (Fig. 3D), which is linked to increased inflammation.

Proteasome dysfunction and buildup of ubiquitinated proteins are linked to increases in inflammation, thus we evaluated tPVAT cytokine production. First, we looked at chemoattractant cytokines because of the increased immune specific gene expression. Cytokine assays showed an increase ($p<0.05$) in both monocyte chemoattractant protein-1 (MCP-1) and chemokine (C-X-C motif) ligand-1 (KC/Gro) (Fig. 4A). Further, all cytokines profiled showed a drastic alteration in OZR compared to LZR, with pro-inflammatory mediators (TNFα, IL-1β, IL-6, IFN-γ, and TSP-1, Fig 4 A&B) significantly elevated and anti-inflammatory mediators (IL-4, IL-5, IL-10, IL-13, and adiponectin, Fig. 4 C&D).

After observing a ~10-fold increase in TNF gene expression and ~10X increase in TNFα secretion in OZR tPVAT, we repeated aortic function experiments with a TNFα-AB to determine its role in orchestrating the observed dysfunction. Additionally, we targeted NOX2 the prominent NOX enzyme of inflammatory immune cells, as it is a known target of TNFα.

PVAT with TNFα Neutralization

Gene Expression—We first sought to determine the role of TNFα on OZR-tPVAT gene expression. TNFα-AB treatment (ex-vivo) significantly down-regulated phosphorylation of nuclear factor kappa-light-chain-enhancer (NF-κB, Fig. 5A), reduced TNF inflammatory gene expression, and decreased gene expression of NOX2 and its regulator p47phox (Fig. 5B). Additionally, TNFα-AB reduced ($p<0.05$) MMP-9 gene expression and increased ($p<0.05$) the gene expression for Nrf2, IL-10, and adiponectin (Fig. 5B), highlighting the role TNFα in the regulation of gene expression in the tPVAT. However, does TNFα-AB treatment ameliorate tPVAT ROS production and the activation of aortic ROS by tPVAT?

ROS—TNFα-AB treatment caused a marked reduction ($p<0.001$) in the DHE signal from OZR-tPVAT to similar levels observed with inhibition by NOX2ds-TAT (Fig. 5C). In turn, the TNFα-AB treatment in OZR-tPVAT completely inhibited the tPVAT activation of ROS in both OZR and LZR aorta ($p<0.001$, Fig. 5C). Further, highlighting the importance of TNFα activation of NOX2 in OZR-tPVAT dysfunction, inhibition with NOX2ds-TAT completely inhibited the tPVAT activation of ROS produced by the aorta ($p<0.001$, Fig. 5C). To determine if the diminished proteasome activity in OZR-tPVAT was acutely mediated by TNFα we cultured OZR-tPVAT with TNFα-AB and ran all 3 proteasome assays. The results showed no effect of TNFα-AB (VMAX: LLYV 1.2±0.05, RLR 2.5±0.07, nLPnLD 0.5±0.04, $p>0.05$).

NO and Aortic Reactivity—With TNFα-AB treatment yielding beneficial effects on gene expression and ROS production we examined its actions on NO and aortic EDD. TNFα-AB treatment in OZR-tPVAT inhibited tPVAT mediated reduction of NO production from OZR and LZR aortas ($p<0.001$, Fig. 5D). In turn, TNFα-AB treatment in OZR-tPVAT completely inhibited tPVAT mediated dysfunction of aortic EDD in both OZR and LZR ($p<0.01$, Fig. 5 E&F). To highlight the importance of NOX2 in the TNFα mediated aortic dysfunction, we treated OZR-tPVAT with NOX2ds-TAT and demonstrated aortic EDD was completely restored ($p<0.001$, Fig. 5E), however the combination of TNFα-AB and NOX2ds-TAT caused no further improvement ($p>0.05$, maximal relaxation: 71±3%). Additionally, the treatment of the aorta (without tPVAT) with TNFα-AB and NOX2ds-TAT had no effects (Max relaxation OZR Ao 68±2%, OZR Ao+TNFα-AB 69±3%, OZR Ao +NOX2ds-TAT 67±2%). To show the importance of tPVAT activation of aortic ROS production, the LZR and OZR aortas were pretreated with TEMPOL, which prevented the impaired EDD ($p<0.05$, maximal relaxation: OZR tPVAT-Ao+TEMPOL 78±2% vs OZR tPVAT-Ao 58±2% vs OZR Ao 68±2%). Our data to this point has established the role of OZR-tPVAT mediating NO regulation of smooth muscle tone, and thus functional aortic stiffness. Additionally, we assessed the role of MetS tPVAT on aortic remodeling and structural stiffness.

Elastic Modulus—Aortic stiffness was increased ($p<0.01$) by ~90% in the OZR compared to LZR (Fig. 6A). Thus, we wanted to examine the role of tPVAT in OZR aortic stiffness. We first examined tPVAT gene expression and found an increased MMP9 expression ($p<0.05$) but no change in MMP2 and TIMP-1 (Fig. 6B). We then examined the aortic protein levels of TIMP-1, which were decreased in OZR compared to the LZR (Fig. 6C). Further, activity levels of MMP9, assessed in tPVAT exudate, were increased in OZR compared to LZR, and treating tPVAT with the TNFα-AB prevented the increase in MMP9 activity (Fig. 6D). This laid the groundwork for the potential role of OZR-tPVAT to affect aortic remodeling. Next we examined the direct contribution of tPVAT to aortic stiffness, and the role of TNFα. Co-culturing the LZR aorta with LZR-tPVAT did not alter the elastic modulus compared to culture control; however, the LZR aorta cultured with OZR-tPVAT showed an increased ($p<0.01$) elastic modulus (Fig. 6E), which was completely inhibited when the LZR aorta with OZR-tPVAT were cultured with the TNFα-AB ($p<0.01$, Fig. 6E).

Discussion

Previous studies have detailed the effect of hypertension and obesity on PVAT function. However, MetS pathology is dependent on the complex interactions of its components and may yield differing effects than a component in isolation. Uncovering the distinct and coordinating signaling pathways of the MetS components in tPVAT warrants future evaluation. Our present study identified key mediators of tPVAT dysfunction and demonstrated an essential role of tPVAT on aortic dysfunction in MetS. We identified, for first time, diminished 20S proteasome activity as a potential mechanism of tPVAT dysfunction in MetS. Additionally, we demonstrated TNFα as a key orchestrator of tPVAT ROS production through a NOX2 dependent pathway, and activation of aortic ROS production through a non-NOX2, NADPH oxidase pathway. Additionally, we demonstrated that both NOX2 ROS and TNFα are essential for the observed aortic dysfunction. Finally, we demonstrated tPVAT from OZR could mediate aortic stiffness through a TNFα dependent mechanism targeting MMP9 activity. Chronic effects and the temporal development of vascular dysfunction in MetS are well defined (Katakam *et al.*, 2006; Donley *et al.*, 2014; Brooks *et al.*, 2015). However, the role of tPVAT in orchestrating aortic function in MetS was previously unknown. Collectively our study has important implications of tPVAT pathological consequences on aortic stiffness in MetS and highlights the potential avenue of adipo-centric therapeutic development.

MetS PVAT Environment

Similar to what has been shown in obesity (Shimizu *et al.*, 2014), our data suggests a phenotypic “whitening” of the MetS tPVAT, supported by the change in UCP-1 expression. Loss of UCP-1 and a white-like phenotype are associated with ROS (Lin *et al.*, 2005) and inflammation (Sakamoto *et al.*, 2013). In the current study the potential phenotypic shift in tPVAT was associated with increased KC/Gro and MCP-1 levels, resulting in increased inflammatory immune cell markers (CD68 and CD8a), which produce TNFα and possess NOX2. Our data from inhibition of the NOX p47phox subunit suggests NOX2 was largely responsible for the tPVAT ROS production. Further, an increased NOX2 activity coupled with a substantial reduction in SOD activity in OZR-tPVAT, likely accounts for the increased

ROS production in tPVAT. Importantly, our data showed TNFα was a key mediator for the elevated ROS in MetS tPVAT. Activation of NOX2 ROS appears to be dependent on TNFα, as the simultaneous treatment with both NOX2ds-TAT and TNFα-AB didn't cause a further reduction in ROS production. This is in line with the literature suggesting multiple TNFα functions are carried out by the activation of NADPH oxidases (Li *et al.*, 2005; Kim *et al.*, 2007). Additionally, the TNFα-AB treatment showed partial restoration of tPVAT gene expression, likely due to direct action on TNFα and subsequent reductions in ROS (Sen & Packer, 1996) resulting in the observed decrease in NF-κB activation. This suggests chronic changes in oxidative and inflammatory machinery might also be driven by TNFα and its activation of NOX2. Interestingly, the inhibition of NOX and/or the use of the TNFα-AB did not completely inhibit ROS production, and ROS levels were still well above those measured in LZR-tPVAT. This highlights the role of other oxidative enzymes, and potentially other cytokine mediators playing some role in tPVAT ROS production.

Recently, both obese human and mouse visceral adipose tissue showed reduced chymotrypsin-like activity in the proteasome and was linked to development of insulin resistance, a hallmark of MetS (Diaz-Ruiz *et al.*, 2015). We wanted to build upon these observations, as tPVAT is more protein dense than visceral adipose tissue, which we speculated would magnify the importance of proteasome function. ROS is known to damage and misfold proteins, which are cleared by the 26S proteasome. The 26S comprises of the 20S core bound to one or two 19S regulatory particles, which feed ubiquitinated and damaged proteins into the 20S core (Smith *et al.*, 2011). Our results showed increased ROS, and for the first time in tPVAT, impaired proteasome function. The accumulation of ubiquitinated proteins was likely due to the loss of proteasome capacity, and therefore the accumulation of proteasomal substrates. Interestingly, diminished proteasome function was not due to the loss of 20S proteasome levels (Fig 2). The increase accumulation of damaged and misfolded proteins can lead to cellular and oxidative stress (Otoda *et al.*, 2013; Ghosh *et al.*, 2015; Hohn *et al.*, 2016). Specifically, buildup of oxidized and ubiquitin proteins through activation of endoplasmic reticulum stress induced production of inflammatory cytokines (Ghosh *et al.*, 2015). Suggesting, proteasome dysfunction may contribute to increased pro-inflammatory cytokine production. Future endeavors will be aimed at assessing the causative and or exacerbating role of the entire ubiquitin-proteasome system in disease mediated PVAT dysfunction.

tPVAT Regulation of Aortic Function

Our data showed a blunted aortic EDD in OZR, which was further reduced in the presence of OZR-tPVAT. The impaired EDD was derived from reduced bioavailability of NO in OZR aorta, which was further reduced (~20%) in the presence of OZR-tPVAT. Pro-inflammatory cytokines and ROS, which were increased in OZR-tPVAT, have the potential to interfere with NO bioavailability (Laursen *et al.*, 2001; Yang & Rizzo, 2007). The acute tPVAT impairment of the aorta was due to OZR-tPVAT derived TNFα inducing aortic ROS. This is supported by TNFα-AB inhibiting OZR-tPVAT impairment of both OZR and LZR aortic EDD and the lack of TNFα-AB effect on OZR aorta without tPVAT EDD. The activation of ROS production (via NOX) can interfere with NO bioavailability (Vasquez-Vivar *et al.*, 1998; Yang & Rizzo, 2007). Our data implicates NOX, but not NOX2, in aortic ROS

production as NOX2ds-TAT had no effect on OZR aorta without tPVAT. This is in opposition to Serpillon et.al. (Serpillon *et al.*, 2009) who showed p47phox inhibition in the aorta caused a profound reduction of ROS. We speculate this difference may be due to the advanced diabetic state of the rats in the previous study (Serpillon *et al.*, 2009) resulting in a shift in oxidative enzymes upon the development of type-2 diabetes, and the influence of advanced glycation end products receptor signaling (Zhang *et al.*, 2006). Our data showed that NOX2 inhibition in OZR-tPVAT had the same impact as TNFα neutralization, suggesting tPVAT impairment of the aorta is dependent on ROS. We therefore, experimentally created an oxidative environment with pyrogallol in healthy tPVAT was unable to recreate the same level of aortic dysfunction as MetS tPVAT. This would suggest the phenotypic changes in MetS tPVAT are essential for the production capacity of inflammatory mediators that activate aortic ROS, and interfere with NO bioavailability.

Previous data has shown that TNFα activates the production of ROS from oxidative enzymes, such as NADPH oxidase (Li *et al.*, 2005; Kim *et al.*, 2007). In our study, we showed the activation of aortic ROS production by OZR tPVAT could be completely abolished by a TNFα-AB. Similarly, albeit in a completely different vascular bed, the small resistance vessels from obese patients showed an increased gene expression of TNF in PVAT, and use of a TNFα receptor inhibitor reduced vessel ROS production (Virdis *et al.*, 2015), but due to experimental design they were unable to differentiate between basal and PVAT activation of ROS. In addition to direct activation of ROS, TNFα mediates expression of IL-1β (Turner *et al.*, 2007), another stimulator of oxidative enzymes (Gurjar *et al.*, 2001). Additionally, IL-1β can act to enhance TNFα signaling through regulation of TNF receptors (Saperstein *et al.*, 2009). This implicates IL-1β in a supportive role to TNFα in mediating OZR-tPVAT regulation of aortic dysfunction. Both TNFα and IL-1β levels can be regulated by IL-10 (Raychaudhuri *et al.*, 2000; Zemse *et al.*, 2010), which we showed to be reduced in exudate from OZR-tPVAT. In addition, IL-10 is a known inhibitor of oxidative enzymes (Didion *et al.*, 2009), which may explain the reduction of OZR aorta ROS following incubation with LZR tPVAT. Suggesting losing IL-10 release from tPVAT removes the brakes from ROS production and exacerbates the increase of inflammatory cytokines in OZR. Finally, our data showed elevated IFN-γ, which has been implicated in PVAT mediation of vascular dysfunction. However, TNFα-AB treatment completely blocked OZR-tPVAT mediated aortic dysfunction and no evidence suggests a role of TNFα in IFN-γ secretion. This suggests IFN-γ secretion may not affect acute aortic function in MetS; however, it may play a role in chronic vascular dysfunction as previously shown (Mikolajczyk *et al.*, 2016).

In addition, MetS altered levels of cytokines with direct impact on NO production. TSP-1, a multifunctional homotrimeric matrix glycoprotein, was released from tPVAT at a higher concentration in OZR than LZR. Importantly, TSP-1 can inhibit eNOS activation and thus reduce NO production (Isenberg *et al.*, 2009). Further, TSP-1 has a direct role in mediating immune infiltration (Mandler *et al.*, 2017), a key source of tissue inflammation. However, TSP-1 expression can also be mediated by TNFα signaling (Fairaq *et al.*, 2015) suggesting a role for TNFα mediating TSP-1 production as a potential mechanism of tPVAT mediated aortic dysfunction in MetS. Another potential mechanism for the reduced NO bioavailability could be the reduced release of adiponectin from OZR-tPVAT. Adiponectin can inhibit

inflammation (Wang *et al.*, 2014) and promote NO production (Wang & Scherer, 2008). This is in concurrence with data showing PVAT derived adiponectin regulates small (100 to 150 μm diameter) peripheral artery function (Greenstein *et al.*, 2009). The chronic loss or TNFα inhibition of adiponectin stimulating (Wang & Scherer, 2008) eNOS gene expression may play a part in the pathological loss of vascular eNOS. The chronic effect of tPVAT derived TNFα on the aorta is beyond the scoop of this study and warrants future investigations.

tPVAT mediated aortic stiffness

In addition to NO regulation of EDD, previous studies have shown NO is an essential regulator of ECM remodeling and aortic structure (Jenkins *et al.*, 1998; Gurjar *et al.*, 1999). In obese and aged mice, tPVAT was shown to increase arterial stiffness through alterations of oxidative status, leading to elastin fragmentation (Chen *et al.*, 2013; Fleenor *et al.*, 2014). However, PVAT may also directly affect ECM remodeling as adipocytes and immune cells express MMPs (Bouloumie *et al.*, 2001; Chakraborti *et al.*, 2003), in particular, MMP9 which is highly associated with aortic stiffness and displays elastase activity (Yasmin *et al.*, 2005). The fragmentation of elastin increases aortic stiffness by causing the loading of collagen fibers at lower pressures (Lakatta & Levy, 2003). tPVAT production of TNFα may play an important role in the aortic stiffening with MetS through a number of pathways. First, TNFα is known to stimulate the production of MMP9 (Wu *et al.*, 2013) and we found that OZR-tPVAT had increased MMP9 activity, which was associated with increased stiffness. Inhibition of TNFα by TNFα-AB treatment decreased both MMP9 activity and aortic stiffness. Second, TNFα can indirectly stimulate MMP9 though its promotion of other cytokines, whereby both IL-1β and TSP-1 can activate MMP9 (Donnini *et al.*, 2004; Brown *et al.*, 2007) and active MMP9 can cleave TNFα (Gearing *et al.*, 1994) and IL-1β into active forms (Schonbeck *et al.*, 1998). Third, ROS has also been implicated in the fragmentation of elastin (Chen *et al.*, 2013; Fleenor *et al.*, 2014), thus TNFα activation of ROS may also play a role in the observed aortic stiffness in our study. Fourth, reduced levels of TIMP-1 (a tissue inhibitor of MMPs) can further add to MMP9 mediated aortic dysfunction (Roderfeld *et al.*, 2007). Further research into a causative effect of tPVAT derived MMPs is warranted.

Clinical Outlook

The findings from the current study may help to elucidate mechanisms underlying increased aortic stiffness. Our data suggests adding treatment for adipose tissue dysfunction to a multifaceted therapeutic approach in MetS may improve vascular function. Our data identifies tPVAT localized NOX2 as an essential component of tPVAT mediated aortic dysfunction. As NOX2 is predominantly found in immune cells (Bedard & Krause, 2007) the development of adipose tissue specific immunotherapy or tissue specific delivery of inhibitors might have potential therapeutic benefits. Lastly, building evidence suggests restoring functionality of the ubiquitin-proteasome system in MetS might restore adipose function and insulin sensitivity (Diaz-Ruiz *et al.*, 2015; Hohn *et al.*, 2016), and our data suggest a potential pleiotropic effect on vascular function.

Limitations

A limitation of our co-culture experiment was the lack of intraluminal flow in the aortic rings, which is an important for shear stress mediated release of NO and regulation of stiffness. However, the use of a media control helps to account for the increase in stiffness due to the lack of flow. Additionally, crossover studies examining the effect of LZR tPVAT co-culture with OZR aortic stiffness were unable to be conducted due to the limited availability of LZR tPVAT. Finally, aortic function experiments were conducted ex-vivo and may not reflect the magnitude of impairment imposed by tPVAT in-vivo. However, many logistical hurdles remain in assessing tPVAT regulation of the aorta in-vivo. We believe our data clearly shows OZR tPVAT can activate aortic ROS and impair aortic function, which warrants future investigations of OZR tPVAT cytokine concentrations in-vivo.

Conclusions

In summary, we are the first to show in MetS a comprehensive picture of tPVAT TNFα production, which regulates gene expression and ROS production (specifically NOX2 derived ROS) in the tPVAT. Additionally, we showed global reductions in proteasome function in MetS tPVAT. These effects of MetS on tPVAT increase the production of TNFα, TSP-1, and IL-1β and decrease production of IL-10 and adiponectin, which leads to a reduction in NO, EDD, MMP9 activity, and increases in structural stiffness. These data suggest that tPVAT dysfunction was a major driving force in MetS aortic impairment and highlights the potential for adipo-centric therapeutics.

Acknowledgments

Funding

This study was supported by the American Heart Association grants IRG14330015, pre-doctoral fellowship AHA (14PRE20380386); National Institute of General Medical Sciences of the National Institutes of Health (U54GM104942, and 5P20GM109098).

We would like to acknowledge Vincent Setola PhD and David Siderovski PhD for assistance with PCR experiments and the use of their Qiagen equipment.

References

Bedard K, Krause KH. The NOX family of ROS-generating NADPH oxidases: physiology and pathophysiology. Physiol Rev. 2007; 87:245–313. [PubMed: 17237347]

Bouloumie A, Sengenes C, Portolan G, Galitzky J, Lafontan M. Adipocyte produces matrix metalloproteinases 2 and 9: involvement in adipose differentiation. Diabetes. 2001; 50:2080–2086. [PubMed: 11522674]

Brooks SD, DeVallance E, d'Audiffret AC, Frisbee SJ, Tabone LE, Shrader CD, Frisbee JC, Chantler PD. Metabolic syndrome impairs reactivity and wall mechanics of cerebral resistance arteries in obese Zucker rats. Am J Physiol Heart Circ Physiol. 2015; 309:H1846–1859. [PubMed: 26475592]

Brown RD, Jones GM, Laird RE, Hudson P, Long CS. Cytokines regulate matrix metalloproteinases and migration in cardiac fibroblasts. Biochem Biophys Res Commun. 2007; 362:200–205. [PubMed: 17706606]

Chakraborti S, Mandal M, Das S, Mandal A, Chakraborti T. Regulation of matrix metalloproteinases: an overview. Mol Cell Biochem. 2003; 253:269–285. [PubMed: 14619979]

Chen JY, Tsai PJ, Tai HC, Tsai RL, Chang YT, Wang MC, Chiou YW, Yeh ML, Tang MJ, Lam CF, Shiesh SC, Li YH, Tsai WC, Chou CH, Lin LJ, Wu HL, Tsai YS. Increased aortic stiffness and attenuated lysyl oxidase activity in obesity. Arterioscler Thromb Vasc Biol. 2013; 33:839–846. [PubMed: 23413430]

Chen XL, Zhang Q, Zhao R, Medford RM. Superoxide, H2O2, and iron are required for TNF-alpha-induced MCP-1 gene expression in endothelial cells: role of Rac1 and NADPH oxidase. Am J Physiol Heart Circ Physiol. 2004; 286:H1001–1007. [PubMed: 14576080]

Diaz-Ruiz A, Guzman-Ruiz R, Moreno NR, Garcia-Rios A, Delgado-Casado N, Membrives A, Tunez I, El Bekay R, Fernandez-Real JM, Tovar S, Dieguez C, Tinahones FJ, Vazquez-Martinez R, Lopez-Miranda J, Malagon MM. Proteasome Dysfunction Associated to Oxidative Stress and Proteotoxicity in Adipocytes Compromises Insulin Sensitivity in Human Obesity. Antioxid Redox Signal. 2015; 23:597–612. [PubMed: 25714483]

Didion SP, Kinzenbaw DA, Schrader LI, Chu Y, Faraci FM. Endogenous interleukin-10 inhibits angiotensin II-induced vascular dysfunction. Hypertension. 2009; 54:619–624. [PubMed: 19620507]

Donley DA, Fournier SB, Reger BL, DeVallance E, Bonner DE, Olfert IM, Frisbee JC, Chantler PD. Aerobic exercise training reduces arterial stiffness in metabolic syndrome. J Appl Physiol (1985). 2014; 116:1396–1404. [PubMed: 24744384]

Donnini S, Morbidelli L, Taraboletti G, Ziche M. ERK1-2 and p38 MAPK regulate MMP/TIMP balance and function in response to thrombospondin-1 fragments in the microvascular endothelium. Life Sci. 2004; 74:2975–2985. [PubMed: 15051421]

Fairaq A, Goc A, Artham S, Sabbineni H, Somanath PR. TNFalpha induces inflammatory stress response in microvascular endothelial cells via Akt- and P38 MAP kinase-mediated thrombospondin-1 expression. Mol Cell Biochem. 2015; 406:227–236. [PubMed: 25963668]

Fitch RM, Vergona R, Sullivan ME, Wang YX. Nitric oxide synthase inhibition increases aortic stiffness measured by pulse wave velocity in rats. Cardiovasc Res. 2001; 51:351–358. [PubMed: 11470475]

Fleenor BS, Eng JS, Sindler AL, Pham BT, Kloor JD, Seals DR. Superoxide signaling in perivascular adipose tissue promotes age-related artery stiffness. Aging Cell. 2014; 13:576–578. [PubMed: 24341314]

Gao YJ, Lu C, Su LY, Sharma AM, Lee RM. Modulation of vascular function by perivascular adipose tissue: the role of endothelium and hydrogen peroxide. Br J Pharmacol. 2007; 151:323–331. [PubMed: 17384669]

Gearing AJ, Beckett P, Christodoulou M, Churchill M, Clements J, Davidson AH, Drummond AH, Galloway WA, Gilbert R, Gordon JL, et al. Processing of tumour necrosis factor-alpha precursor by metalloproteinases. Nature. 1994; 370:555–557. [PubMed: 8052310]

Ghosh AK, Garg SK, Mau T, O'Brien M, Liu J, Yung R. Elevated Endoplasmic Reticulum Stress Response Contributes to Adipose Tissue Inflammation in Aging. J Gerontol A Biol Sci Med Sci. 2015; 70:1320–1329. [PubMed: 25324219]

Greenstein AS, Khavandi K, Withers SB, Sonoyama K, Clancy O, Jeziorska M, Laing I, Yates AP, Pemberton PW, Malik RA, Heagerty AM. Local inflammation and hypoxia abolish the protective anticontractile properties of perivascular fat in obese patients. Circulation. 2009; 119:1661–1670. [PubMed: 19289637]

Gurjar MV, Deleon J, Sharma RV, Bhalla RC. Role of reactive oxygen species in IL-1 beta-stimulated sustained ERK activation and MMP-9 induction. Am J Physiol Heart Circ Physiol. 2001; 281:H2568–2574. [PubMed: 11709424]

Gurjar MV, Sharma RV, Bhalla RC. eNOS gene transfer inhibits smooth muscle cell migration and MMP-2 and MMP-9 activity. Arterioscler Thromb Vasc Biol. 1999; 19:2871–2877. [PubMed: 10591663]

Hohn A, Konig J, Jung T. Metabolic Syndrome, Redox State, and the Proteasomal System. Antioxid Redox Signal. 2016; 25:902–917. [PubMed: 27412984]

Isenberg JS, Martin-Manso G, Maxhimer JB, Roberts DD. Regulation of nitric oxide signalling by thrombospondin 1: implications for anti-angiogenic therapies. Nat Rev Cancer. 2009; 9:182–194. [PubMed: 19194382]

Jenkins GM, Crow MT, Bilato C, Gluzband Y, Ryu WS, Li Z, Stetler-Stevenson W, Nater C, Froehlich JP, Lakatta EG, Cheng L. Increased expression of membrane-type matrix metalloproteinase and preferential localization of matrix metalloproteinase-2 to the neointima of balloon-injured rat carotid arteries. Circulation. 1998; 97:82–90. [PubMed: 9443435]

Katakam PV, Snipes JA, Tulbert CD, Mayanagi K, Miller AW, Busija DW. Impaired endothelin-induced vasoconstriction in coronary arteries of Zucker obese rats is associated with uncoupling of [Ca2+]i signaling. Am J Physiol Regul Integr Comp Physiol. 2006; 290:R145–153. [PubMed: 16322351]

Kim YS, Morgan MJ, Choksi S, Liu ZG. TNF-induced activation of the Nox1 NADPH oxidase and its role in the induction of necrotic cell death. Mol Cell. 2007; 26:675–687. [PubMed: 17560373]

Lakatta EG, Levy D. Arterial and cardiac aging: major shareholders in cardiovascular disease enterprises: Part I: aging arteries: a “set up” for vascular disease. Circulation. 2003; 107:139–146. [PubMed: 12515756]

Laursen JB, Somers M, Kurz S, McCann L, Warnholtz A, Freeman BA, Tarpey M, Fukai T, Harrison DG. Endothelial regulation of vasomotion in apoE-deficient mice: implications for interactions between peroxynitrite and tetrahydrobiopterin. Circulation. 2001; 103:1282–1288. [PubMed: 11238274]

Levy BI, Ambrosio G, Pries AR, Struijker-Boudier HA. Microcirculation in hypertension: a new target for treatment? Circulation. 2001; 104:735–740. [PubMed: 11489784]

Li JM, Fan LM, Christie MR, Shah AM. Acute tumor necrosis factor alpha signaling via NADPH oxidase in microvascular endothelial cells: role of p47phox phosphorylation and binding to TRAF4. Mol Cell Biol. 2005; 25:2320–2330. [PubMed: 15743827]

Lin Y, Berg AH, Iyengar P, Lam TK, Giacca A, Combs TP, Rajala MW, Du X, Rollman B, Li W, Hawkins M, Barzilai N, Rhodes CJ, Fantus IG, Brownlee M, Scherer PE. The hyperglycemia-induced inflammatory response in adipocytes: the role of reactive oxygen species. J Biol Chem. 2005; 280:4617–4626. [PubMed: 15536073]

Mandler WK, Nurkiewicz TR, Porter DW, Olfert IM. Thrombospondin-1 mediates multi-walled carbon nanotube induced impairment of arteriolar dilation. Nanotoxicology. 2017; 11:112–122. [PubMed: 28024456]

Mikolajczyk TP, Nosalski R, Szczepaniak P, Budzyn K, Osmenda G, Skiba D, Sagan A, Wu J, Vinh A, Marvar PJ, Guzik B, Podolec J, Drummond G, Lob HE, Harrison DG, Guzik TJ. Role of chemokine RANTES in the regulation of perivascular inflammation, T-cell accumulation, and vascular dysfunction in hypertension. FASEB J. 2016; 30:1987–1999. [PubMed: 26873938]

Mingorance C, Alvarez de Sotomayor M, Jimenez-Palacios FJ, Callejon Mochon M, Casto C, Marhuenda E, Herrera MD. Effects of chronic treatment with the CB1 antagonist, rimonabant on the blood pressure, and vascular reactivity of obese Zucker rats. Obesity (Silver Spring). 2009; 17:1340–1347. [PubMed: 19553924]

O’Rourke M. Arterial stiffness, systolic blood pressure, and logical treatment of arterial hypertension. Hypertension. 1990; 15:339–347. [PubMed: 2180816]

Otoda T, Takamura T, Misu H, Ota T, Murata S, Hayashi H, Takayama H, Kikuchi A, Kanamori T, Shima KR, Lan F, Takeda T, Kurita S, Ishikura K, Kita Y, Iwayama K, Kato K, Uno M, Takeshita Y, Yamamoto M, Tokuyama K, Iseki S, Tanaka K, Kaneko S. Proteasome dysfunction mediates obesity-induced endoplasmic reticulum stress and insulin resistance in the liver. Diabetes. 2013; 62:811–824. [PubMed: 23209186]

Parameswaran N, Patial S. Tumor necrosis factor-alpha signaling in macrophages. Crit Rev Eukaryot Gene Expr. 2010; 20:87–103. [PubMed: 21133840]

Raychaudhuri B, Fisher CJ, Farver CF, Malur A, Drazba J, Kavuru MS, Thomassen MJ. Interleukin 10 (IL-10)-mediated inhibition of inflammatory cytokine production by human alveolar macrophages. Cytokine. 2000; 12:1348–1355. [PubMed: 10975994]

Roderfeld M, Graf J, Giese B, Salguero-Palacios R, Tschuschner A, Muller-Newen G, Roeb E. Latent MMP-9 is bound to TIMP-1 before secretion. Biol Chem. 2007; 388:1227–1234. [PubMed: 17976016]

Saji N, Kimura K, Shimizu H, Kita Y. Association between silent brain infarct and arterial stiffness indicated by brachial-ankle pulse wave velocity. Intern Med. 2012; 51:1003–1008. [PubMed: 22576377]

Sakamoto T, Takahashi N, Sawaragi Y, Naknukool S, Yu R, Goto T, Kawada T. Inflammation induced by RAW macrophages suppresses UCP1 mRNA induction via ERK activation in 10T1/2 adipocytes. Am J Physiol Cell Physiol. 2013; 304:C729–738. [PubMed: 23302779]

Saperstein S, Chen L, Oakes D, Pryhuber G, Finkelstein J. IL-1beta augments TNF-alpha-mediated inflammatory responses from lung epithelial cells. J Interferon Cytokine Res. 2009; 29:273–284. [PubMed: 19231998]

Schonbeck U, Mach F, Libby P. Generation of biologically active IL-1 beta by matrix metalloproteinases: a novel caspase-1-independent pathway of IL-1 beta processing. J Immunol. 1998; 161:3340–3346. [PubMed: 9759850]

Sen CK, Packer L. Antioxidant and redox regulation of gene transcription. FASEB J. 1996; 10:709–720. [PubMed: 8635688]

Serpillon S, Floyd BC, Gupte RS, George S, Kozicky M, Neito V, Recchia F, Stanley W, Wolin MS, Gupte SA. Superoxide production by NAD(P)H oxidase and mitochondria is increased in genetically obese and hyperglycemic rat heart and aorta before the development of cardiac dysfunction. The role of glucose-6-phosphate dehydrogenase-derived NADPH. Am J Physiol Heart Circ Physiol. 2009; 297:H153–162. [PubMed: 19429815]

Shimizu I, Aprahamian T, Kikuchi R, Shimizu A, Papanicolaou KN, MacLauchlan S, Maruyama S, Walsh K. Vascular rarefaction mediates whitening of brown fat in obesity. J Clin Invest. 2014; 124:2099–2112. [PubMed: 24713652]

Smith DM, Fraga H, Reis C, Kafri G, Goldberg AL. ATP binds to proteasomal ATPases in pairs with distinct functional effects, implying an ordered reaction cycle. Cell. 2011; 144:526–538. [PubMed: 21335235]

Turner NA, Mughal RS, Warburton P, O'Regan DJ, Ball SG, Porter KE. Mechanism of TNFalpha-induced IL-1alpha, IL-1beta and IL-6 expression in human cardiac fibroblasts: effects of statins and thiazolidinediones. Cardiovasc Res. 2007; 76:81–90. [PubMed: 17612514]

Vasquez-Vivar J, Kalyanaraman B, Martasek P, Hogg N, Masters BS, Karoui H, Tordo P, Pritchard KA Jr. Superoxide generation by endothelial nitric oxide synthase: the influence of cofactors. Proc Natl Acad Sci U S A. 1998; 95:9220–9225. [PubMed: 9689061]

Virdis A, Duranti E, Rossi C, Dell'Agnello U, Santini E, Anselmino M, Chiarugi M, Taddei S, Solini A. Tumour necrosis factor-alpha participates on the endothelin-1/nitric oxide imbalance in small arteries from obese patients: role of perivascular adipose tissue. Eur Heart J. 2015; 36:784–794. [PubMed: 24578389]

Wang Y, Wang X, Lau WB, Yuan Y, Booth D, Li JJ, Scalia R, Preston K, Gao E, Koch W, Ma XL. Adiponectin inhibits tumor necrosis factor-alpha-induced vascular inflammatory response via caveolin-mediated ceramidase recruitment and activation. Circ Res. 2014; 114:792–805. [PubMed: 24397980]

Wang ZV, Scherer PE. Adiponectin, cardiovascular function, and hypertension. Hypertension. 2008; 51:8–14. [PubMed: 17998473]

Wilkinson IB, Franklin SS, Cockcroft JR. Nitric oxide and the regulation of large artery stiffness: from physiology to pharmacology. Hypertension. 2004; 44:112–116. [PubMed: 15262901]

Wu HT, Sie SS, Kuan TC, Lin CS. Identifying the regulative role of NF-kappaB binding sites within promoter region of human matrix metalloproteinase 9 (mmp-9) by TNF-alpha induction. Appl Biochem Biotechnol. 2013; 169:438–449. [PubMed: 23224948]

Yang B, Rizzo V. TNF-alpha potentiates protein-tyrosine nitration through activation of NADPH oxidase and eNOS localized in membrane rafts and caveolae of bovine aortic endothelial cells. Am J Physiol Heart Circ Physiol. 2007; 292:H954–962. [PubMed: 17028163]

Yasmin, McEniery CM, Wallace S, Dakham Z, Pulsalkar P, Maki-Petaja K, Ashby MJ, Cockcroft JR, Wilkinson IB. Matrix metalloproteinase-9 (MMP-9), MMP-2, and serum elastase activity are associated with systolic hypertension and arterial stiffness. Arterioscler Thromb Vasc Biol. 2005; 25:372. [PubMed: 15556929]

Zemse SM, Chiao CW, Hilgers RH, Webb RC. Interleukin-10 inhibits the in vivo and in vitro adverse effects of TNF-alpha on the endothelium of murine aorta. Am J Physiol Heart Circ Physiol. 2010; 299:H1160–1167. [PubMed: 20639218]

Zhang M, Kho AL, Anilkumar N, Chibber R, Pagano PJ, Shah AM, Cave AC. Glycated proteins stimulate reactive oxygen species production in cardiac myocytes: involvement of Nox2 (gp91phox)-containing NADPH oxidase. Circulation. 2006; 113:1235–1243. [PubMed: 16505175]

New Findings

- What is the central question of this study?
- TNFα has been shown to impair vascular function, however, the impact of tPVAT derived TNFα on tPVAT and aortic function in MetS is unknown.
- What is the main finding and its importance?
- tPVAT release of TNFα causes tPVAT ROS production through activation of NOX2 dependent pathway, activates aortic ROS production, and mediates aortic stiffness potentially through MMP-9 activity. Neutralization of TNFα and or the inhibition of NOX2 blocks the tPVAT impairment of aortic function. These data partly implicate tPVAT NOX2 and TNFα in mediating the vascular pathology of MetS.

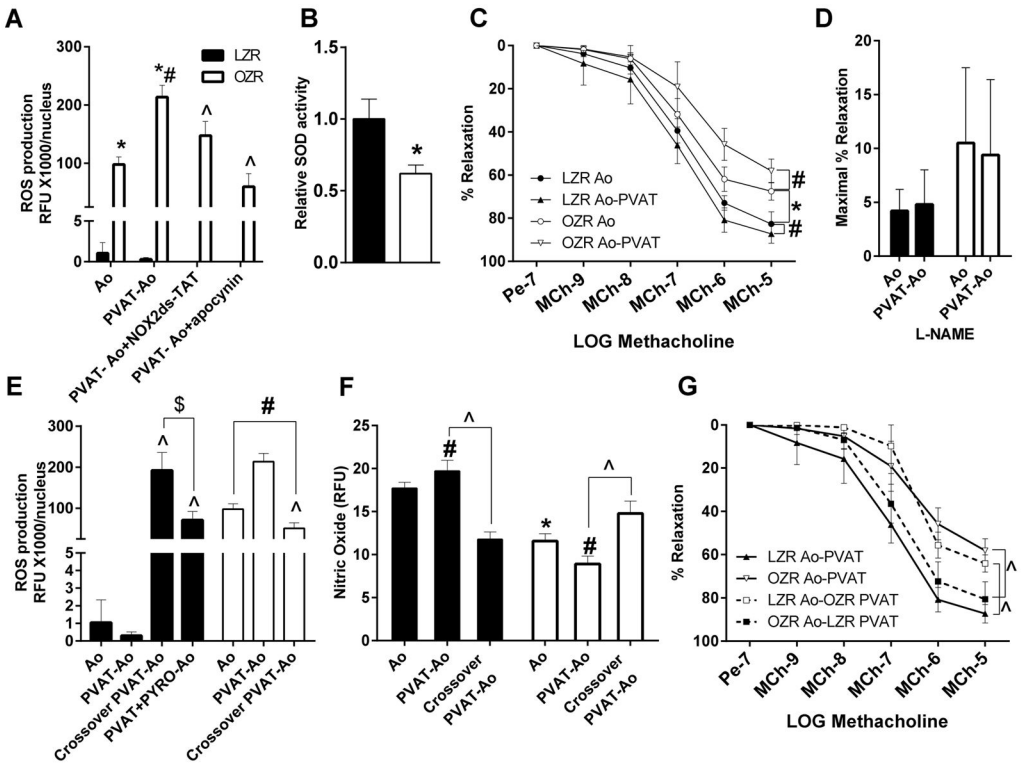

Figure 1. OZR-tPVAT role in activating aortic ROS production and reducing nitric oxide

Effect of tPVAT on A) on aortic (Ao) ROS production, with specific and non-specific inhibition of NADPH oxidases, (n=8, LZR vs OZR compared by t-test and within group effect assessed by repeat measures) was determined by incubating LZR aortas with LZR tPVAT and OZR aortas with OZR tPVAT. B) Relative total SOD activity of aortic homogenates (n=4, assessed by t-test). C) Effect of tPVAT (LZR Ao with LZR tPVAT and OZR Ao with OZR tPVAT) on aortic EDD (n=16, assessed by repeated measures) and maximal relaxation in the presence of the NO inhibitor L-NAME (n=4–8, Ao vs Ao-tPVAT assessed by paired t-test). E, F, & G) To further assess the role of tPVAT on aortic function crossover experiments (LZR Ao with OZR-tPVAT and OZR Ao with LZR-tPVAT) were conducted to determine tPVAT effect on aortic ROS, NO, and EDD (n=8, assessed by repeated measures, 1F LZR Ao vs OZR Ao assessed by t-test). Data expressed as Mean±SD. *denotes significance between LZR and OZR, #denotes a significant difference between tPVAT and Ao within group, and ^denotes a significant difference of drug treatment compared to respective tPVAT. Pe, Phenylephrine; MCh, Methacholine; PYRO, pyrogallol.

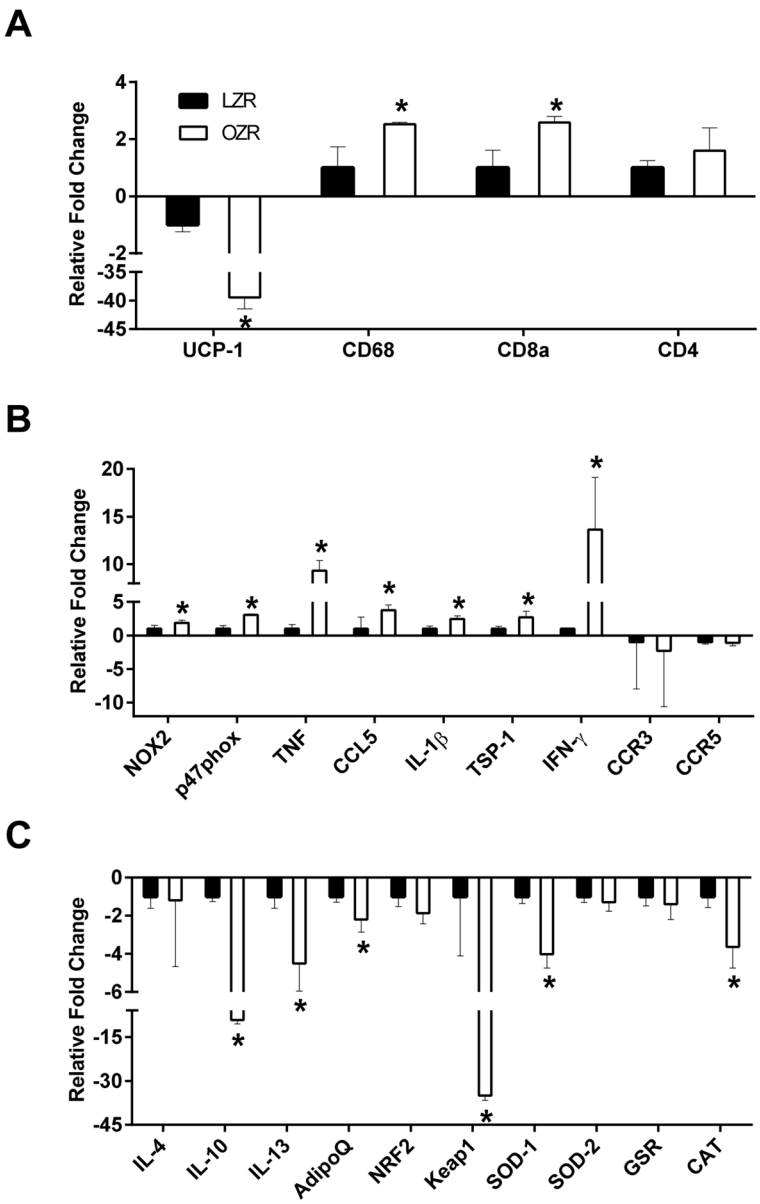

Figure 2. Relative gene expression of tPVAT

Relative gene expression of OZR tPVAT compared to LZR tPVAT for A) phenotype and immune markers, B) oxidative and inflammatory genes, and C) and anti-inflammatory and oxidative defense markers. Data expressed as Mean±SD, *denotes significant difference in OZR vs. LZR, minimum of 2-fold change and t-test $p<0.05$, n=3. UCP-1, uncoupling protein-1; CD, cluster of differentiation; NOX2, NADPH oxidase 2 catalytic subunit (GP91); p47phox, NADPH oxidase 2 intracellular regulatory subunit; TNF, tumor necrosis factor; CCL5, Chemokine (C-C motif) ligand 5; IL, interleukin; TSP-1, thrombospondin 1; IFN-γ, interferon gamma; CCR, C-C motif chemokine receptor; AdipoQ, adiponectin; NFR2, nuclear factor (erythroid 2)-like 2; Keap1, kelch-like ECH associated protein 1, SOD, superoxide dismutase; GSR, glutathione reductase; CAT, catalase.

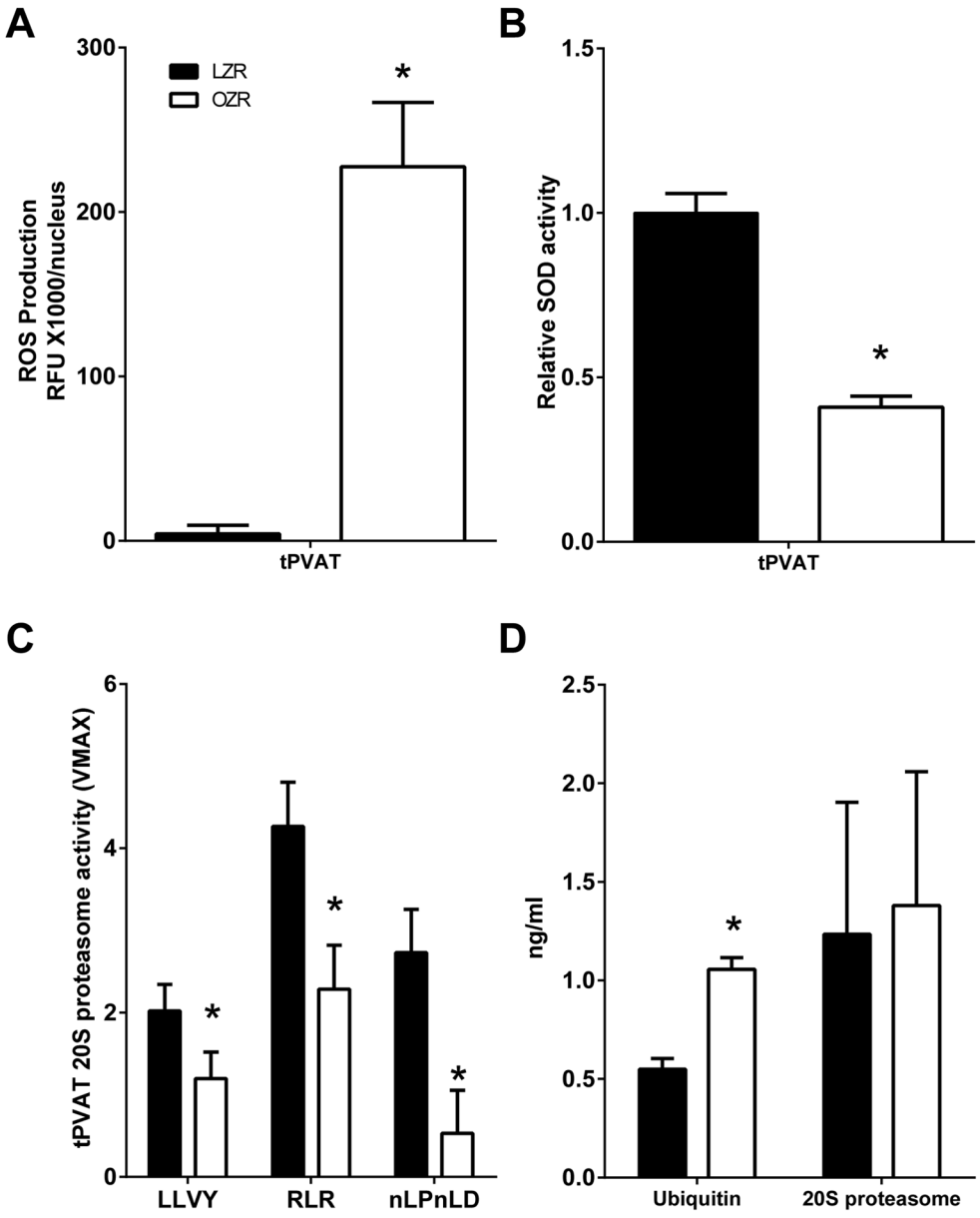

Figure 3. tPVAT ROS formation SOD defense and proteasome function

tPVAT function was assessed by measuring A) ROS production (n=8), B) relative SOD activity (n=5), C) proteasome function, measured across all 3 active sites (n=8, each site was assessed independently by t-test); LLVY (chymotrypsin-like), RLR (trypsin-like) and nLPnLD (peptidylglutamyl-peptide hydrolyzing), and D) levels of ubiquitin and the 20S proteasome from tPVAT homogenates (n=5). Data expressed as Mean±SD, *denotes significant difference in OZR vs. LZR measured by t-test, $p<0.05$.

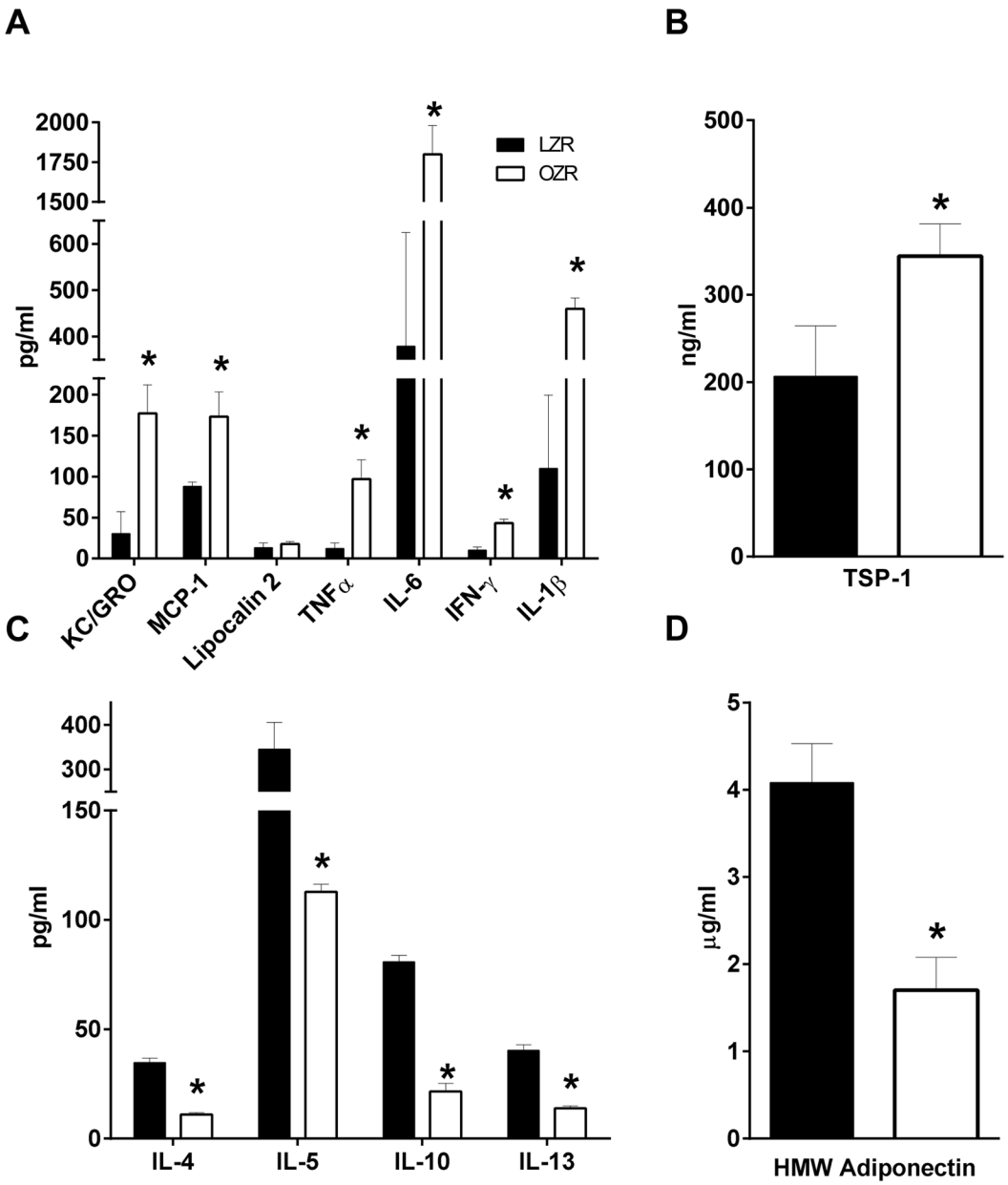

Figure 4. Cytokine profile of tPVAT

The secretion profile of tPVAT exudate was assessed for A & B) immuno-attractive cytokines, inflammatory cytokines, and C & D) anti-inflammatory cytokines (n=5). Data expressed as Mean±SD *denotes a statistically significant change in OZR vs. LZR determined by t-test, $p<0.05$. KC/GRO, chemokine (C-C motif) ligand 1; MCP-1, monocyte chemoattractant protein-1; TNFα, tumor necrosis factor alpha; IL, interleukin; IFN-γ, interferon gamma; TSP-1, thrombospondin 1; HMW adiponectin, high molecular weight adiponectin

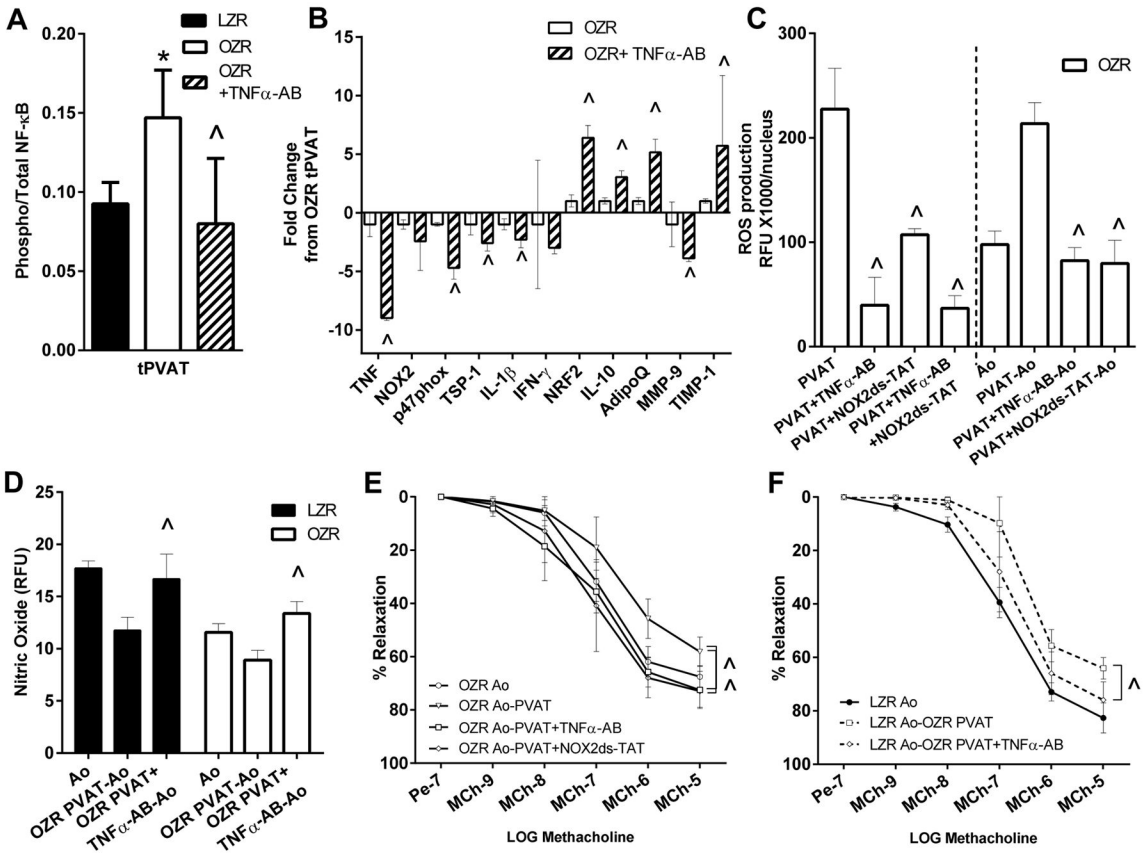

Figure 5. Effect of TNFα-AB on tPVAT and tPVAT mediated aortic function

A) Effect of ex-vivo TNFα-AB treatment on activation of NF-κB in tPVAT shown as the ratio of phosphor:total (n=6), and B) the effect on tPVAT gene expression compared to untreated OZR tPVAT (n=3). Following the ex-vivo treatment of OZR tPVAT with TNFα-AB, NOX2ds-TAT or a combination C) ROS production was assessed in tPVAT and aorta incubated with tPVAT (n=8, repeated measures were used to assess the effect of treatment on tPVAT ROS and separately on the effect of aortic ROS, separation of analysis shown by dashed line). The effect of ex-vivo TNFα-AB treatment on OZR-tPVAT mediated D) NO production and E&F) EDD in OZR aorta and the crossover experiment in LZR aorta (n=5–8). Data expressed as Mean±SD. ^denotes significant effect of treatment compared to control assessed by repeated measures ANOVA, $p<0.05$. Pe, Phenylephrine; MCh, Methacholine; TNF, tumor necrosis factor; NOX2, NADPH oxidase 2 catalytic subunit (GP91); p47phox, NADPH oxidase 2 intracellular regulatory subunit; TSP-1, thrombospondin 1; IL, interleukin; IFN-γ, interferon gamma; NFR2, nuclear factor (erythroid 2)-like 2; AdipoQ, adiponectin MMP, matrix metalloproteinase; TIMP, tissue inhibitor of metalloproteinase.

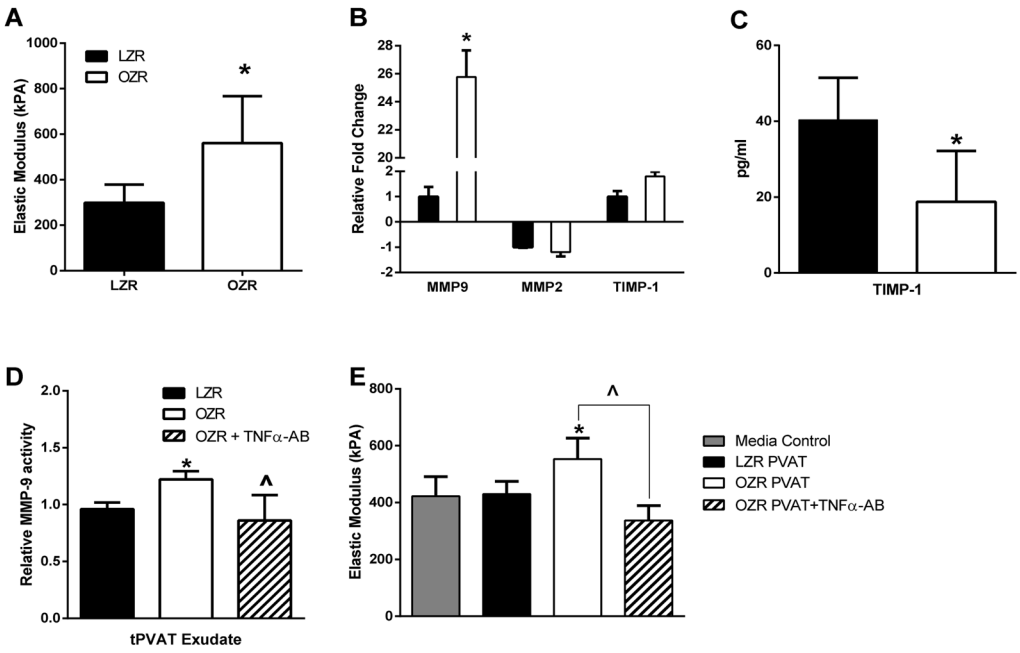

Figure 6. Role of tPVAT in aortic stiffness

Aortic stiffness measured by A) elastic modulus in LZR and OZR rings without culture experiments (n=8, assessed by t-test). Aortic stiffness associated remodeling factors were assessed in tPVAT by B) gene expression (n=3, assessed by t-test), and C) tPVAT tissue levels of TIMP-1 (n=5, assessed by t-test. Additionally, the relative activity of MMP9 form LZR, OZR, and OZR+TNFα-AB tPVAT exudate was measured (n=5, assessed by one-ANOVA). To test the direct effect of tPVAT on aortic stiffness E) elastic modulus of donor LZR aortic rings were measured following 72-hours in culture with media, LZR-tPVAT, OZR-tPVAT, or OZR-tPVAT+TNFα-AB (n= 3–4, assessed by repeated measures ANOVA). Data expressed as Mean±SD. *denotes significant change between OZR and LZR and ^denotes significant effect of TNFα-AB treatment compared to OZR. Statistical significance was set at $p<0.05$. MMP, matrix metalloproteinase; TIMP, tissue inhibitor of metallo-proteinase; TNFα-AB, Tumor necrosis factor alpha neutralizing antibody.